Photoinduced ligand exchange dynamics of a polypyridyl ruthenium complex in aqueous solution

Dixon, I.M.; Bonnet, S.A.; Alary, F.; Cuny, J.

THE JOURNAL OF PHYSICAL CHEMISTRY LETTERS
A JOURNAL OF THE AMERICAN CHEMICAL SOCIETY

pubs.acs.org/JPCL

Letter

Photoinduced Ligand Exchange Dynamics of a Polypyridyl Ruthenium Complex in Aqueous Solution

Isabelle M. Dixon, Sylvestre Bonnet, Fabienne Alary,* and Jérôme Cuny*

Cite This: *J. Phys. Chem. Lett.* 2021, 12, 7278−7284

Read Online

ACCESS | Metrics & More | Article Recommendations | Supporting Information

ABSTRACT: The understanding of photoinduced ligand exchange mechanisms in polypyridyl ruthenium(II) complexes operating in aqueous solution is of crucial importance to rationalize their photoreactivity. Herein, we demonstrate that a synergetic use of ab initio molecular dynamics simulations and static calculations, both conducted at the DFT level, can provide a full understanding of photosubstitution mechanisms of a monodentate ligand by a solvent water molecule in archetypal ruthenium complexes in explicit water. The simulations show that the photoinduced loss of a monodentate ligand generates an unreactive 16-electron species in a hitherto undescribed pentacoordinated triplet excited state that converts, via an easily accessible crossing point, to a reactive 16-electron singlet ground state, which combines with a solvent water molecule to yield the experimentally observed aqua complex in less than 10 ps. This work paves the way for the rational design of novel photoactive metal complexes relevant for biological applications.

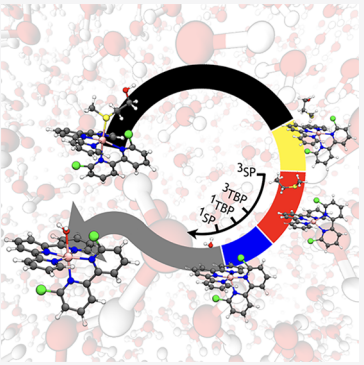

Photoluminescence and photoreactivity processes in polypyridyl ruthenium(II) complexes have attracted considerable attention because of their potential use in biological (light-activatable anticancer compounds)[1−6] or technological (solar cells, molecular machines) applications.[7−11] This family of compounds stands out for its remarkable visible light absorption and emission properties due to low-lying metal-to-ligand charge transfer (MLCT) states which, following ultrafast and nearly quantitative intersystem crossing to their ^{3}MLCT counterparts,[12−14] luminesce in the visible region with lifetimes up to the microsecond.[15] d^6 metal complexes of this family are also characterized by the existence of metal-centered (MC) excited states, resulting from d−d excitation. The accessibility of ^{3}MC states opens several deactivation channels other than ^{3}MLCT photoluminescence, particularly nonradiative deactivation toward reactant and photodegradation through ligand loss processes.[16] However, despite the fundamental importance of understanding their photoreactivity and the vast amount of experimental data collected in recent years, mechanistic details of photosubstitution processes remain unclear.[17−28] Such reactions are difficult to model quantitatively as they typically involve several intercrossing electronic states and different time scales, leading to a scarce number of theoretical mechanistic studies on the photoreactivity itself.[29−36] Among them, a large majority deals with the early stage of the photosubstitution reaction, i.e., the photolabilization of the departing ligand, while none of them have addressed the detailed mechanism of formation of the solvent-bound photoproduct. In the particular case of a series of $[Ru(tpy)(N{-}N)(Hmte)]^{2+}$ complexes (tpy = 2,2′:6′,2″-terpyridine, N−N = bpy (2,2′-bipyridine), biq (2,2′-biquinoline), dcbpy (6,6′-dichloro-2,2′-bipyridine),dmbpy (6,6′-dimethyl-2,2′-bipyridine), Hmte = 2-methylthioethanol), a recent static DFT study, which focused on the first steps of the mechanism leading to thioether photolabilization,[37] has shown that the quantum yield of photosubstitution can be rationalized by the existence of two successive nearly degenerate triplet metal-centered (^{3}MC) isomers sharing the same electronic structure. The first one, named hereafter $^3(Ru)^{MC_{hexa}}_{Hmte}$, is related to the reactant through a close-lying minimum-energy crossing point (MECP), while the second one, named hereafter $^3(Ru)^{MC_{penta}-18}_{Hmte}$, displays an almost pentacoordinate geometry even though the Hmte ligand is still weakly coordinated. $^3(Ru)^{MC_{penta}-18}_{Hmte}$, which still can be viewed as an 18-electron complex, was inferred to lead to the photoproduct following diffusion of the departing Hmte and capture of a solvent water molecule. However, this second part of the mechanism was still hypothetical and, like in all previous studies on this type of reaction, no quantitative information was provided. Limitations of static DFT approaches to describe bulk solvent with a continuum model,[38,39] their difficulties to simulate complicated multistep reaction pathways without any preconditioning, and their inability to describe diffusion processes render a realistic description of the bond-forming part of the photosubstitution reactions out of reach.

In contrast, ab initio molecular dynamics (AIMD) provides an efficient framework to complement the static formalism in order

Received: May 3, 2021
Accepted: July 9, 2021
Published: July 29, 2021

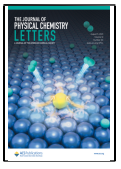

Scheme 1. Schematic Representation of the Different Steps Involved in the Photosubstitution Mechanism of a Thioether Ligand by a Solvent Water Molecule in the Sterically Hindered Complex $[Ru(tpy)(dcbpy)(Hmte)]^{2+}$[a]

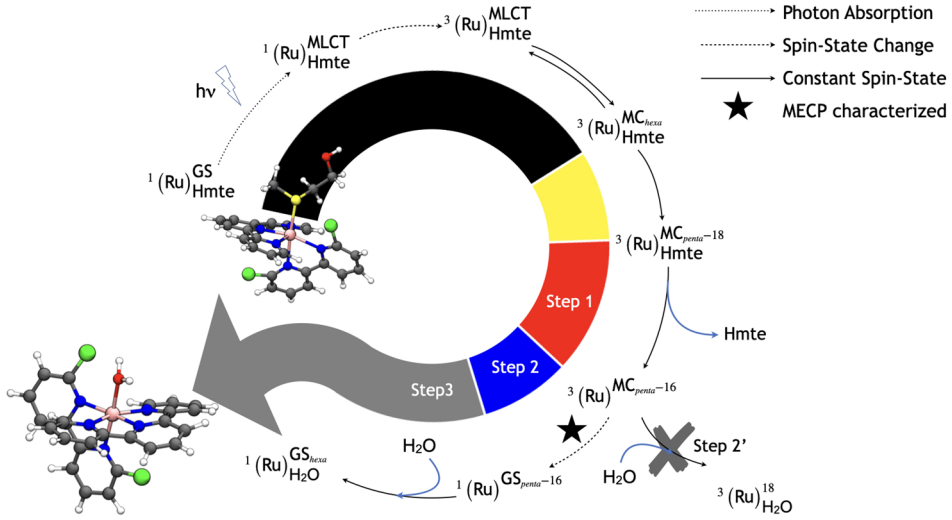

[a]The black and yellow ribbons represent the photorelease steps investigated in ref 37 using static approaches. The yellow ribbon step is revisited in the present study from an AIMD point a view as discussed in the text. Red, blue, and gray ribbons represent the steps presently studied using a combination of AIMD and NEB calculations. Labels in the colored ribbons are the step numbers used in the text to describe the photosubstitution reaction.

to study the events associated with the water and Hmte degrees of freedom in both the ground and excited states. AIMD has been intensively used to study thermal ligand substitution reactions on transition-metal complexes.[40−44] In contrast, to the best of our knowledge, very few AIMD simulations on photoexcited Ru complexes have been conducted, most of them focusing on photophysical properties, without any chemical reaction being involved.[45−47] Herein, we provide a full description of the photosubstitution process in its totality, using explicit solvent molecules and taking into account both ground and excited states to properly understand at which stage, i.e., on which energy surface, the coordination of the incoming ligand is likely to occur. We focus on the $[Ru(tpy)(dcbpy)(Hmte)]^{2+}$ complex as it was shown to display both $^3(Ru)^{MC_{hexa}}_{Hmte}$ and $^3(Ru)^{MC_{penta}-18}_{Hmte}$ states, the latter being proposed as central in the substitution mechanism.[37]

Scheme 1 summarizes the elementary steps involved, as deduced from AIMD simulations and supported by nudged elastic band (NEB) calculations (computational details are provided in Methods). Details of all the molecular and electronic structures and relative energies of the various minima and MECPs in the multistep process are collected in the Supporting Information (Tables S1−S10 and Figures S1−S11), as is the PBE static computation of the states along the yellow ribbon (Figures S12−S14).

It is well-established that photoexcitation initially produces a singlet metal-to-ligand charge transfer (^{1}MLCT) state, $^1(Ru)^{MLCT}_{Hmte}$, which relaxes by intersystem crossing (ISC) to a ^{3}MLCT state, $^3(Ru)^{MLCT}_{Hmte}$ (black ribbon in Scheme 1). The $^3(Ru)^{MC_{hexa}}_{Hmte}$ state can then be populated and will further lead to dissociation by populating a $^3(Ru)^{MC_{penta}-18}_{Hmte}$ state (yellow ribbon in Scheme 1). $^3(Ru)^{MC_{hexa}}_{Hmte}$ could also deactivate nonradiatively to repopulate the reactant ground state (this nonproductive pathway is outside the scope of the present work).[37] From an AIMD point of view, starting from an equilibrated 75 ps simulation of $^1(Ru)^{GS}_{Hmte}$ inserted in a unit cell containing 103 water molecules from which initial conditions were randomly extracted, switching

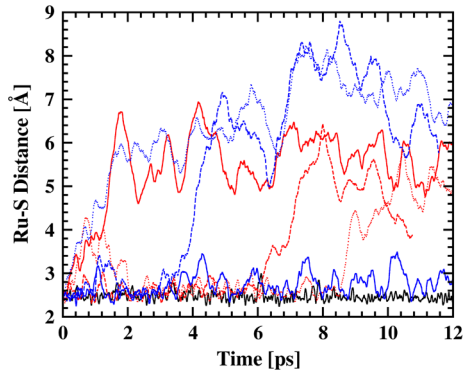

Figure 1. Time evolution of Ru−S distance during AIMD simulations consisting of 103 water molecules and one $^1(Ru)^{GS}_{Hmte}$ (black plain line; canonical simulation) or one $^3(Ru)_{Hmte}$ (blue and red lines; microcanonical simulations) complex. In the former case, the simulation is 75 ps long, although only the first 12 ps are displayed. The average Ru−S distance over the whole simulation is 2.45 Å, which is slightly larger than the value obtained from static geometry optimization (2.40 Å; see Table S1 and Figure S1), and the standard deviation is 0.08 Å. When switching to the lowest-energy triplet state, fluctuations of the Ru−S distance increase significantly and the Hmte ligand can move further from the complex as fast as ∼1 ps. Only one simulation does not lead to dissociation before 12 ps (blue plain line).

to the lowest-energy triplet state potential energy surface (^{3}PES) led to the fast departure of the Hmte ligand. This is highlighted in Figure 1, which compares the time evolution of the Ru−S distance during AIMD simulations performed on the singlet and lowest-energy triplet states. It shows that among the six microcanonical simulations that have been conducted, five lead to dissociation in less than 12 ps, two of them in ∼1 ps, and only one does not, although significant increase of the Ru−S bond length fluctuations is observed, which suggests that dissociation is likely to occur in a short range of time. Figure S15 shows the same behavior during an additional simulation performed on the lowest-energy triplet state in the canonical ensemble.

https://doi.org/10.1021/acs.jpclett.1c01424
J. Phys. Chem. Lett. 2021, 12, 7278−7284

To identify the electronic nature of the triplet state that leads to dissociation, a more detailed analysis of the electronic structure of the visited configurations has been performed. To do so, among the thousands of geometries sampled during the AIMD simulation of $^{1}(Ru)^{GS}_{Hmte}$, 100 were randomly chosen. PBE single-point energy calculations, of the complex only, at these geometries turned out to correspond to 54 ^{3}MC and 46 ^{3}MLCT states. This shows that from a large number of initial conditions, i.e., configurations, extracted from the singlet ground-state simulation, the lowest-energy state reached on the ^{3}PES can be either $^{3}(Ru)^{MLCT}_{Hmte}$ or $^{3}(Ru)^{MC}_{Hmte}$ states, with a slightly higher propensity for the latter one. It is worth noting that because of the rather short Ru−S distances of the configurations visited in the ground-state simulation (see black curve in Figure 1) these ^{3}MC states are mainly of the $^{3}(Ru)^{MC_{hexa}}_{Hmte}$ type. Once in the triplet state, 100 configurations were randomly selected along the canonical AIMD simulation performed in the triplet state, before dissociation, and subject to PBE single-point energy calculations. These configurations are all of the $^{3}(Ru)^{MC}_{Hmte}$ type. All these results show that, at that stage, structural deformations resulting from thermal fluctuations make the distinction between the $^{3}(Ru)^{MLCT}_{Hmte}$, $^{3}(Ru)^{MC_{hexa}}_{Hmte}$, and $^{3}(Ru)^{MC_{penta}-18}_{Hmte}$ states difficult to make. The frontier between black, yellow, and red ribbons of Scheme 1 is intrinsically less defined at the AIMD level than in the static calculations of Göttle et al.[37] $^{3}(Ru)^{MC_{penta}-18}_{Hmte}$ can therefore be seen as a transient state as there is no evidence that the system can be trapped in this particular state for a significant amount of time. With this in mind and focusing on the coordination process (red, blue, and gray ribbons in Scheme 1), the photosubstitution mechanism can be formalized into four possible steps:

- **Step 1**: Diffusion of the Hmte ligand and formation of a 16-electron intermediate $^{3}(Ru)^{MC_{penta}-16}$ (red ribbon, characterized using AIMD simulations).
- **Step 2′**: Coordination of water on $^{3}(Ru)^{MC_{penta}-16}$ and generation of the aqua product in a triplet state $^{3}(Ru)^{18}_{H_2O}$.
- **Step 2**: Spin crossover from $^{3}(Ru)^{MC_{penta}-16}$ to a closed-shell singlet 16-electron complex $^{1}(Ru)^{GS_{penta}-16}$ (blue ribbon, characterized using static calculations).
- **Step 3**: Coordination of water on $^{1}(Ru)^{GS_{penta}-16}$ to form the aqua product in a singlet state (gray ribbon, characterized using AIMD simulations).

Step 1 can be described by the six microcanonical simulations performed on the lowest-energy triplet states presented in Figure 1. As stated above, as soon as spin multiplicity is switched to three, the Hmte ligand is likely to dissociate and diffuse from the ruthenium center as the sulfur atom is found ∼5 Å from it in less than 12 ps in five of these simulations. This is all the more true when the AIMD simulations start from a predissociated state characterized by a Ru−S distance of 3.8 Å, as found in $^{3}(Ru)^{MC_{penta}-18}$. In that case, the sulfur atom of the Hmte ligand is found ∼5−9 Å from the Ru atom in less than 7 ps, as shown in Figure S16. **Step 1** releases a 16-electron complex called $^{3}(Ru)^{MC_{penta}-16}$. Strikingly, no subsequent approach and accordingly no coordination of a water molecule was observed, as highlighted by the pair radial distribution functions $g_{Ru-O}(r)$ presented in Figure S17. They show that after dissociation, whatever the considered simulation, no water molecule comes closer than 3.6 Å to the ruthenium atom. Even this particular incursion below 4 Å is unique and appears to be transient, so that all the water molecules are located at least 4 Å from the ruthenium atom. This thereby excludes the occurrence of **Step 2′** during the time frame of these simulations.

To better understand the absence of reactivity between $^{3}(Ru)^{MC_{penta}-16}$ and solvent molecules, we further examined the conformational fluctuations occurring during the release of the Hmte ligand (**Step 1**). As shown in Figure 2, the Ru(II)

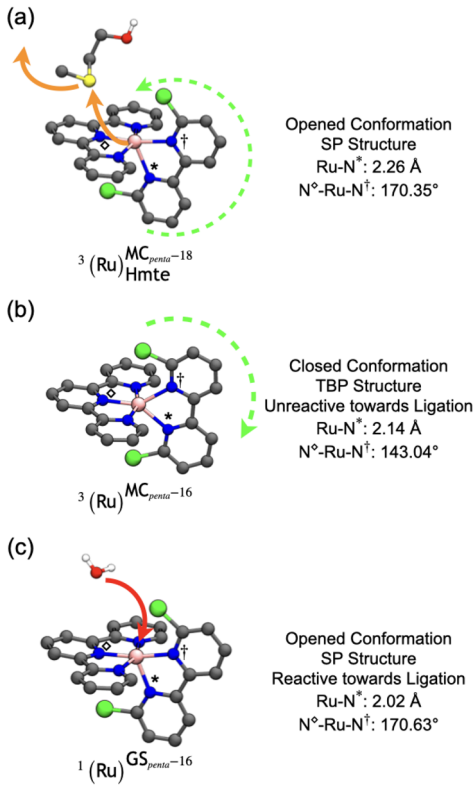

Figure 2. Schematic representation of the intramolecular rearrangements occurring in the key species involved in ligand exchange. (a) Diffusion of the Hmte ligand and closing of the dcbpy ligand (**Step 1**). (b) Opening of the dcbpy ligand (end of **Step 2**) and (c) binding of a water molecule (**Step 3**). Distances and angles are from the static DFT-optimized minima.

coordination sphere is strongly modified after ligand departure, relaxing to a trisbipyramidal- (TBP) like structure (Figure 2b). In this state, the Ru−N* bond *trans* to the dissociation coordinate shrinks from 2.26 to 2.14 Å and hence recovers a value similar to that encountered in the reactant ground state (2.13 Å). Most importantly this shrinking of Ru−N* is accompanied by a tilting of the bipyridine ligand leading to a closed TBP geometry, which prevents the subsequent approach and binding of a water molecule (**Step 2′**, not observed). Geometry optimization and frequency analysis of $^{3}(Ru)^{MC_{penta}-16}$ in TBP geometry confirm the local minimum nature of this state on the ^{3}PES. Figure S18 also displays the time evolution of the $N^{\diamond}-Ru-N^{\dagger}$ angle along the five microcanonical simulations of Figure 1 leading to dissociation. In four of them, tilting of the bipyridine ligand occurs in a few picoseconds following Hmte departure. As an additional proof of the unreactive character of this species, a simulation consisting of one $^{3}(Ru)^{MC_{penta}-16}$ complex solvated by 110 water molecules was conducted during 46 ps. Again, no coordination of water occurred with $^{3}(Ru)^{MC_{penta}-16}$, which remained in its TBP geometry throughout, highlighting the lack of reactivity of this species toward the surrounding water molecules. This is in line with the 77 ps measured by

https://doi.org/10.1021/acs.jpclett.1c01424
J. Phys. Chem. Lett. 2021, 12, 7278−7284

Turro and co-workers for the quenching of a pentacoordinate $^3Ru(bpy)_2(CH_3CN)^{2+}$ complex by water.[20]

To further proceed to water ligation, and as the triplet state seemed poorly prone to bind water, we investigated an alternative route involving reactivity on the closed-shell ^{1}PES. In this scenario, the MECP allowing for the hopping between surfaces has been scrutinized using a static approach (**Step 2**). The MECP and $^3(Ru)^{MC_{penta}-16}$ were found to be quasi-degenerate, with an energy difference around 0.38 kJ mol^{-1} (4 meV), and they both displayed the same closed TBP structure (Figure S8). Therefore, we further investigated reactivity occurring on the singlet surface.

Starting from the MECP structure, geometry optimization in the singlet closed-shell state leads to $^1(Ru)^{GS_{penta}-16}$ (end of **Step 2**). During geometry optimization, the bipyridine ligand rotates around the same axis as that of **Step 1** (Figure 2a), resulting in a quasi-square pyramidal (SP) opened conformation (Figure 2c). This $^1(Ru)^{GS_{penta}-16}$ species bears an electron deficiency on the metal, making it a strong electrophile at the ruthenium center, and is now "sterically" free to interact with a water molecule.[48] In parallel, four AIMD simulations of the singlet state close to the MECP geometry, i.e., as closed ^{1}TBP, lead to the $^1(Ru)^{GS_{penta}-16}$ intermediate in its opened SP geometry. This intramolecular rearrangement (end of **Step 2**) and coordination of a water molecule (**Step 3**) occur in less than 10 ps (Figure 3) and lead to

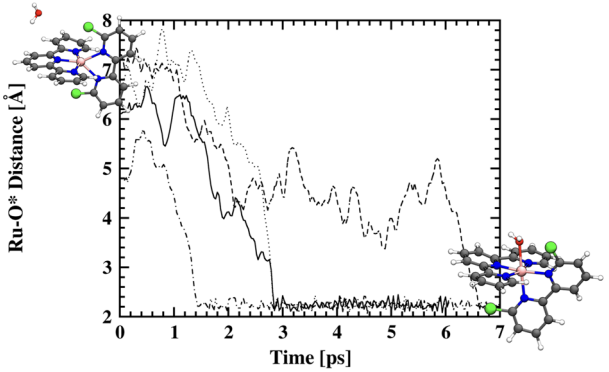

Figure 3. Water capture in the singlet state as illustrated by the Ru−O* distance along the four simulations performed in the singlet state from initial conditions extracted from the canonical AIMD simulation of the $^3(Ru)^{MC_{penta}-16}$ complex (**Step 3**). O* refers to the oxygen atom of the incoming water molecule.

the final aqua complex $[Ru(tpy)(dcbpy)(H_2O)]^{2+}$ in its ground state. Similar observations, i.e., ^{1}TBP →^{1}SP relaxation followed by water capture, can be made from NEB calculations corresponding to the approach of one water molecule toward ^{1}TBP (Figure S19).

The proposed reaction pathway requires both spin conversion and conformational changes between TBP and SP geometries. Our investigations echo the experimental results obtained on the photoaquation of $[Fe(CN_6)]^{4-}$ by Chergui et al.,[49] which evidenced fast ligand loss followed by slow ligand capture. In our case, we relate the latter to the conformational trapping in an unreactive TBP triplet state. Spin crossing to the singlet TBP structure is shown to be a key event that triggers, following evolution toward a reactive SP singlet state, coordination of the entering water molecule.

To conclude, by combining AIMD and static methods, both conducted at the DFT level, we report a theoretical study that reveals for the first time the photoaquation pathway and time frame of $[Ru(tpy)(dcbpy)(Hmte)]^{2+}$ by considering reactivity along both adiabatic and nonadiabatic pathways. This work demonstrates that populating a ^{3}MC state in solution can lead to dissociation of the Hmte ligand. Additionally, and most importantly, the release of the monodentate ligand produces a pentacoordinate ^{3}MC state, in which structural rearrangements prevent the coordination of a solvent molecule by adopting a TBP-like structure, disfavoring the formation of the aqua product in the triplet state. Upon spin conversion to the singlet, the TBP-like species undergoes a conformational change and evolves to an electrophilic SP-like structure that frees access to an incoming water molecule, leading to the facile barrierless formation of the aqua product. These findings do not suffer from any simplification of the solvent description as AIMD allows us to explicitly take its contribution into account. Although the present study focuses primarily on the mechanism occurring at and near the metal center, one can hypothesize that the detailed structure of the hydrogen bond network around the complex, which can be impacted by the nature of the polypyridyl ligands, could play a role on the time scale of the recombination step. However, such detailed analysis would require a significant amount of additional simulations to converge the hydrogen bond network behavior, which is highly statistical in nature. The observed entanglement between spin state and reactivity toward ligand exchange (as in two-state reactivity)[50] is reminiscent of metalloenzyme reactivity. Such elementary steps could be extended to photosubstitution mechanisms in other transition-metal complexes. In addition, as the SP-to-TBP relaxation observed following ligand loss in the triplet state seems to delay the capture of the entering ligand, one could anticipate that tuning relaxation to the TBP geometry with appropriate substituent effects could be of help to foster the overall efficiency of the process and thus improve biological applications of polypyridyl ruthenium(II) complexes.

METHODS

Static DFT Calculations. All the calculations were performed at the density functional theory (DFT) level using the Orca 3.0 program package.[51] Calculations were performed using the Perdew−Burke−Ernzerhof functional (PBE)[52] to be consistent with the AIMD simulations. It is worth noting that the present PBE results are also fully consistent with the PBE0[53] results previously reported in terms of energy ordering and energy gaps reported by Göttle et al. (see Table S11).[37] We used a triple-ζ quality basis set including one polarization function for C, N, O, S, Cl, and Ru atoms (Ahlrichs Def2-TZVP(-f)) and a double-ζ quality basis set also including one polarization function for hydrogen atoms (Ahlrichs Def2-SVP).[54] All geometry optimizations, minimum-energy crossing points (MECP) optimizations, and frequency calculations used the conductor-like screening model (COSMO) to simulate the water solvent.[55] Minimum-energy paths (MEPs) were optimized using the nudged elastic band (NEB) method using the module developed by Paulette Clancy's group interfaced with ORCA 3.0.[56,57] Convergence criterion for NEB calculation was set to 0.05 eV/Å. The number of beads used in NEB calculations was adjusted to fit the transformation. These calculations were performed using the BFGS and FIRE algorithms in the presence of COSMO.

Ab Initio Molecular Dynamics Simulations. AIMD simulations were performed within the Car−Parrinello formalism as implemented in the CPMD code v. 3.17.[58,59] The exchange−correlation interaction was described using the PBE functional.[52] Generalized gradient approximated (GGA) functionals such as PBE are known to lead to an overstructured and frozen-like liquid

https://doi.org/10.1021/acs.jpclett.1c01424
J. Phys. Chem. Lett. 2021, 12, 7278−7284

water compared to the experiments. In particular, Sit and Marzari demonstrated that PBE liquid water displays a frozen-like character below 400 K and a liquid-like character above.[60] Thus, to overcome this limitation, we chose to perform all the simulations at 400 K to conserve a proper liquid-like character of the solvent, as performed elsewhere.[61] Electronic wave functions and densities were expanded with a plane-wave basis-set defined by an energy cutoff of 35 and 280 Ry, respectively. Valence-core interactions were described by use of ultrasoft pseudopotentials.[62] For Ru, the valence included the 4s, 4p, 4d, and 5s states. The Koelling−Harmon scalar relativistic equation was solved for the initial all-electron calculation of the Ru pseudopotential generation. The Brillouin zone integration was done at the Γ-point only.

All simulations of $[Ru(tpy)(dcbpy)(Hmte)]^{2+}$ consisted of 103 heavy water molecules and one complex in a 16.5 × 16.5 × 16.5 Å^3 cubic box. For simulations in the canonical ensemble, a colored-noise Langevin thermostat was especially designed for CPMD simulations and tuned to optimally sample all the frequencies of the system up to 800 cm^{-1}.[63] The initial configuration of the water molecules was generated from a 25 ps AIMD simulation of pure water performed at 400 K at the ambient density. The $^1(Ru)^{GS}_{Hmte}$ complex, the configuration of which was obtained from a static PBE calculation, was then added by hand in the simulation box that was then equilibrated in the canonical ensemble during 16 ps prior to a 75 ps production simulation in the singlet ground state. A time step of 0.1 fs and a fictitious electron mass parameter of 400 au were employed in all singlet-state simulations. The six simulations performed in the lowest-energy triplet state presented in Figure 1 were performed in the microcanonical ensemble starting from initial conditions randomly selected along the aforementioned singlet ground-state simulation. They were 12 ps long each. A time step of 0.075 fs was used in combination with a fictitious electron mass parameter of 400 au. These parameters were also used in all subsequent simulations performed in the triplet state. All simulations performed in the triplet state were done by fixing the spin multiplicity to 3, which imposes that all such simulations evolve on the lowest-energy triplet state potential energy surface.

Simulation of the $^3(Ru)^{MC_{penta}-16}$ complex consisted of 110 heavy water molecules and one complex. The initial structure was constructed using one frame randomly taken from one of the dissociation simulations from which the Hmte ligand was removed and replaced by seven water molecules. An equilibration run of 10 ps was performed prior to 46 ps of a production run in the lowest-energy triplet state. The four recombination trajectories presented in Figure 3 were performed in the singlet state, in the microcanonical ensemble, from four sets of initial conditions extracted from the aforementioned simulation of $^3(Ru)^{MC_{penta}-16}$.

■ ASSOCIATED CONTENT

Supporting Information

The Supporting Information is available free of charge at https://pubs.acs.org/doi/10.1021/acs.jpclett.1c01424.

Coordinates of the $^1(Ru)^{GS}_{Hmte}$, $^3(Ru)^{MLCT}_{Hmte}$, $^3(Ru)^{MC_{hexa}}_{Hmte}$, $^3(Ru)^{MC_{penta}-18}_{Hmte}$, $^3(Ru)^{MC_{penta}-16}$, $^1(Ru)^{GS_{penta}-16}$, and $^1(Ru)^{GS_{hexa}}_{H_2O}$ complexes optimized at the PBE level; structure of the MECPs $^3(Ru)^{MC_{hexa}}_{Hmte} \rightarrow {}^1(Ru)^{GS}_{Hmte}$, $^{1/3}(Ru)^{MC_{penta}-18}_{Hmte}$, and $^{1/3}(Ru)^{MC_{penta}-16}$ optimized at the PBE level; MEPs between $^3(Ru)^{MLCT}_{Hmte}$ and $^3(Ru)^{MC_{hexa}}_{Hmte}$, $^3(Ru)^{MLCT}_{Hmte}$ and $^3(Ru)^{MC_{penta}-18}_{Hmte}$, $^3(Ru)^{MC_{hexa}}_{Hmte}$ and $^3(Ru)^{MC_{penta}-18}_{Hmte}$, and MECP$(^{1/3}(Ru)^{MC_{penta}-16})$ + H_2O and $^1(Ru)^{GS_{hexa}}_{H_2O}$; Jablonski diagram and a comparison between PBE and PBE0 energies and energy gaps; time evolution of Ru−S distance during a canonical simulation following simulation of $^1(Ru)^{GS}_{Hmte}$; time evolution of Ru−S distance from seven microcanonical simulations starting from predissociated state; $g_{Ru-O}(r)$ pair radial distribution functions; and time evolution of $N^{\diamond}$−Ru−$N^{\dagger}$ angle (PDF)

■ AUTHOR INFORMATION

Corresponding Authors

Fabienne Alary − *Université de Toulouse, CNRS, Université Toulouse III - Paul Sabatier, Laboratoire de Chimie et Physique Quantiques, 31062 Toulouse, France;* orcid.org/0000-0003-4154-0815; Email: fabienne.alary@irsamc.ups-tlse.fr

Jérôme Cuny − *Université de Toulouse, CNRS, Université Toulouse III - Paul Sabatier, Laboratoire de Chimie et Physique Quantiques, 31062 Toulouse, France;* orcid.org/0000-0002-7882-9156; Email: jerome.cuny@irsamc.ups-tlse.fr

Authors

Isabelle M. Dixon − *Université de Toulouse, CNRS, Université Toulouse III - Paul Sabatier, Laboratoire de Chimie et Physique Quantiques, 31062 Toulouse, France;* orcid.org/0000-0001-5551-6715

Sylvestre Bonnet − *Leiden Institute of Chemistry, Leiden University, 2300 RA Leiden, The Netherlands;* orcid.org/0000-0002-5810-3657

Complete contact information is available at: https://pubs.acs.org/10.1021/acs.jpclett.1c01424

Notes

The authors declare no competing financial interest.

■ ACKNOWLEDGMENTS

The authors thank the supercomputing facility of Toulouse University, CALMIP, for the allocation of computer resources (Projects P1320, P0059, and P18013). This work was also performed using HPC resources from GENCI-CINES (Grant 2015-x2015087429).

■ REFERENCES

(1) Farrer, N. J.; Salassa, L.; Sadler, P. J. Photoactivated Chemotherapy (PACT): The Potential of Excited-State d-Block Metals in Medicine. *Dalton Trans.* **2009**, 10690−10701.

(2) Schatzschneider, U. Photoactivated Biological Activity of Transition-Metal Complexes. *Eur. J. Inorg. Chem.* **2010**, *2010*, 1451−1467.

(3) Howerton, B. S.; Heidary, D. K.; Glazer, E. C. Strained Ruthenium Complexes Are Potent Light-Activated Anticancer Agents. *J. Am. Chem. Soc.* **2012**, *134*, 8324−8327.

(4) Mari, C.; Pierroz, V.; Ferrari, S.; Gasser, G. Combination of Ru(II) Complexes andLight: New Frontiers in Cancer Therapy. *Chem. Sci.* **2015**, *6*, 2660−2686.

(5) Lameijer, L. N.; Ernst, D.; Hopkins, S. L.; Meijer, M. S.; Askes, S. H. C.; Le Dévédec, S. E.; Bonnet, S. A Red-Light-Activated Ruthenium-Caged NAMPT Inhibitor Remains Phototoxic in Hypoxic Cancer Cells. *Angew. Chem., Int. Ed.* **2017**, *56*, 11549−11553.

(6) van Rixel, V. H. S.; Ramu, V.; Auyeung, A. B.; Beztsinna, N.; Leger, D. Y.; Lameijer, L. N.; Hilt, S. T.; le Dévédec, S. E.; Yildiz, T.; Betancourt, T.; et al. Photo-Uncaging of a Microtubule-Targeted

Rigidin Analogue in Hypoxic Cancer Cells and in a Xenograft Mouse Model. *J. Am. Chem. Soc.* **2019**, *141*, 18444−18454.
(7) Gill, M. R.; Garcia-Lara, J.; Foster, S. J.; Smythe, C.; Battaglia, G.; Thomas, J. A. A Ruthenium(II) Polypyridyl Complex for Direct Imaging of DNA Structure in Living Cells. *Nat. Chem.* **2009**, *1*, 662−667.
(8) Liu, Z.; He, W.; Guo, Z. Metal Coordination in Photoluminescent Sensing. *Chem. Soc. Rev.* **2013**, *42*, 1568−1600.
(9) Pashaei, B.; Shahroosvand, H.; Graetzel, M.; Nazeeruddin, M. K. Influence of Ancillary Ligands in Dye-Sensitized Solar Cells. *Chem. Rev.* **2016**, *116*, 9485−9564.
(10) Colasson, B.; Credi, A.; Ragazzon, G. Light-Driven Molecular Machines based on Ruthenium(II) Polypyridine Complexes: Strategies and Recent Advances. *Coord. Chem. Rev.* **2016**, *325*, 125−134.
(11) Saygili, Y.; Stojanovic, M.; Flores-Díaz, N.; Zakeeruddin, S. M.; Vlachopoulos, N.; Grätzel, M.; Hagfeldt, A. Metal Coordination Complexes as Redox Mediators in Regenerative Dye-Sensitized Solar Cells. *Inorganics* **2019**, *7*, 30.
(12) Damrauer, N. H.; Cerullo, G.; Yeh, A.; Boussie, T. R.; Shank, C. V.; McCusker, J. K. Femtosecond Dynamics of Excited-State Evolution in $[Ru(bpy)_3]^{2+}$. *Science* **1997**, *275*, 54−57.
(13) Atkins, A. J.; González, L. Trajectory Surface-Hopping Dynamics Including Intersystem Crossing in $[Ru(bpy)_3]^{2+}$. *J. Phys. Chem. Lett.* **2017**, *8*, 3840−3845.
(14) Penfold, T. J.; Gindensperger, E.; Daniel, C.; Marian, C. M. Spin-Vibronic Mechanism for Intersystem Crossing. *Chem. Rev.* **2018**, *118*, 6975−7025.
(15) Juris, A.; Balzani, V.; Barigelletti, F.; Campagna, S.; Belser, P.; von Zelewsky, A. Ru(II) Polypyridine Complexes: Photophysics, Photochemistry, Eletrochemistry, and Chemiluminescence. *Coord. Chem. Rev.* **1988**, *84*, 85−277.
(16) Soupart, A.; Alary, F.; Heully, J.-L.; Elliott, P. I.; Dixon, I. M. Recent progress in ligand photorelease reaction mechanisms: Theoretical insights focusing on Ru(II) ^{3}MC states. *Coord. Chem. Rev.* **2020**, *408*, 213184.
(17) Bahreman, A.; Limburg, B.; Siegler, M. A.; Bouwman, E.; Bonnet, S. Spontaneous Formation in the Dark, and Visible Light-Induced Cleavage, of a Ru-S Bond in Water: A Thermodynamic and Kinetic Study. *Inorg. Chem.* **2013**, *52*, 9456−9469.
(18) Gabrielsson, A.; Záliš, S.; Matousek, P.; Towrie, M.; Vlček, A. Ultrafast Photochemical Dissociation of an Equatorial CO Ligand from trans(X,X)-$[Ru(X)_2(CO)_2(bpy)]$ (X = Cl, Br, I): A Picosecond Time-Resolved Infrared Spectroscopic and DFT Computational Study. *Inorg. Chem.* **2004**, *43*, 7380−7388.
(19) Petroni, A.; Slep, L. D.; Etchenique, R. Ruthenium(II) 2,2'-Bipyridyl Tetrakis Acetonitrile Undergoes Selective Axial Photocleavage. *Inorg. Chem.* **2008**, *47*, 951−956.
(20) Liu, Y.; Turner, D. B.; Singh, T. N.; Angeles-Boza, A. M.; Chouai, A.; Dunbar, K. R.; Turro, C. Ultrafast Ligand Exchange: Detection of a Pentacoordinate Ru(II) Intermediate and Product Formation. *J. Am. Chem. Soc.* **2009**, *131*, 26−27.
(21) Borfecchia, E.; Garino, C.; Gianolio, D.; Salassa, L.; Gobetto, R.; Lamberti, C. Monitoring Excited State Dynamics in cis-$[Ru(bpy)_2(py)_2]^{2+}$ by Ultrafast Synchrotron Techniques. *Catal. Today* **2014**, *229*, 34−45.
(22) Camilo, M. R.; Cardoso, C. R.; Carlos, R. M.; Lever, A. B. P. Photosolvolysis of cis-$[Ru(\alpha\text{-diimine})_2(4\text{-aminopyridine})_2]^{2+}$ Complexes: Photophysical, Spectroscopic, and Density Functional Theory Analysis. *Inorg. Chem.* **2014**, *53*, 3694−3708.
(23) Wachter, E.; Glazer, E. C. Mechanistic Study on the Photochemical "Light Switch" Behavior of $[Ru(bpy)_2dmdppz]^{2+}$. *J. Phys. Chem. A* **2014**, *118*, 10474−10486.
(24) Word, T. A.; Whittington, C. L.; Karolak, A.; Kemp, M. T.; Woodcock, H. L.; van der Vaart, A.; Larsen, R. W. Photoacoustic Calorimetry Study of Ligand Photorelease from the Ru(II)bis(2,2'-bipyridine)(6,6'-dimethyl-2,2'-bipyridine) Complex in Aqueous Solution. *Chem. Phys. Lett.* **2015**, *619*, 214−218.
(25) Scattergood, P. A.; Khushnood, U.; Tariq, A.; Cooke, D. J.; Rice, C. R.; Elliott, P. I. P. Photochemistry of $[Ru(pytz)(btz)_2]^{2+}$ and Characterization of a κ^1-btz Ligand-Loss Intermediate. *Inorg. Chem.* **2016**, *55*, 7787−7796.
(26) Kubeil, M.; Vernooij, R. R.; Kubeil, C.; Wood, B. R.; Graham, B.; Stephan, H.; Spiccia, L. Studies of Carbon Monoxide Release from Ruthenium(II) Bipyridine Carbonyl Complexes upon UV-Light Exposure. *Inorg. Chem.* **2017**, *56*, 5941−5952.
(27) Loftus, L. M.; Li, A.; Fillman, K. L.; Martin, P. D.; Kodanko, J. J.; Turro, C. Unusual Role of Excited State Mixing in the Enhancement of Photoinduced Ligand Exchange in Ru(II) Complexes. *J. Am. Chem. Soc.* **2017**, *139*, 18295−18306.
(28) White, J. K.; Schmehl, R. H.; Turro, C. An Overview of Photosubstitution Reactions of Ru(II) Imine Complexes and their Application in Photobiology and Photodynamic Therapy. *Inorg. Chim. Acta* **2017**, *454*, 7−20.
(29) Ding, L.; Chung, L. W.; Morokuma, K. Excited-State Proton Transfer Controls Irreversibility of Photoisomerization in Mononuclear Ruthenium(II) Monoaquo Complexes: A DFT Study. *J. Chem. Theory Comput.* **2014**, *10*, 668−675.
(30) Tu, Y.-J.; Mazumder, S.; Endicott, J. F.; Turro, C.; Kodanko, J. J.; Schlegel, H. B. Selective Photodissociation of Acetonitrile Ligands in Ruthenium Polypyridyl Complexes Studied by Density Functional Theory. *Inorg. Chem.* **2015**, *54*, 8003−8011.
(31) Soupart, A.; Alary, F.; Heully, J.-L.; Elliott, P. I. P.; Dixon, I. M. Exploration of Uncharted ^{3}PES Territory for $[Ru(bpy)_3]^{2+}$: A New ^{3}MC Minimum Prone to Ligand Loss Photochemistry. *Inorg. Chem.* **2018**, *57*, 3192−3196.
(32) Dixon, I. M.; Heully, J.-L.; Alary, F.; Elliott, P. I. P. Theoretical Illumination of Highly Original Photoreactive ^{3}MC States and the Mechanism of the Photochemistry of Ru(II) tris(bidentate) Complexes. *Phys. Chem. Chem. Phys.* **2017**, *19*, 27765−27778.
(33) Salassa, L.; Garino, C.; Salassa, G.; Gobetto, R.; Nervi, C. Mechanism of Ligand Photodissociation in Photoactivable $[Ru(bpy)_2L_2]^{2+}$ Complexes: A Density Functional Theory Study. *J. Am. Chem. Soc.* **2008**, *130*, 9590−9597.
(34) Nisbett, K.; Tu, Y.-J.; Turro, C.; Kodanko, J. J.; Schlegel, H. B. DFT Investigation of Ligand Photodissociation in $[Ru^{II}(tpy)(bpy)(py)]^{2+}$ and $[Ru^{II}(tpy)(Me2bpy)(py)]^{2+}$ Complexes. *Inorg. Chem.* **2018**, *57*, 231−240.
(35) Greenough, S. E.; Roberts, G. M.; Smith, N. A.; Horbury, M. D.; McKinlay, R. G.; Żurek, J. M.; Paterson, M. J.; Sadler, P. J.; Stavros, V. G. Ultrafast Photo-Induced Ligand Solvolysis of cis-$[Ru(bipyridine)_2(nicotinamide)_2]^{2+}$: Experimental and Theoretical insight into its Photoactivation Mechanism. *Phys. Chem. Chem. Phys.* **2014**, *16*, 19141−19155.
(36) Kayanuma, M.; Shoji, M.; Shigeta, Y. Photosubstitution Reaction of cis-$[Ru(bpy)_2(CH_3CN)_2]^{2+}$ and cis-$[Ru(bpy)_2(NH_3)_2]^{2+}$ in Aqueous Solution via Monoaqua Intermediate. *J. Phys. Chem. A* **2019**, *123*, 2497−2502.
(37) Göttle, A. J.; Alary, F.; Boggio-Pasqua, M.; Dixon, I. M.; Heully, J.-L.; Bahreman, A.; Askes, S. H. C.; Bonnet, S. Pivotal Role of a Pentacoordinate ^{3}MC State on the Photocleavage Efficiency of a Thioether Ligand in Ruthenium(II) Complexes: A Theoretical Mechanistic Study. *Inorg. Chem.* **2016**, *55*, 4448−4456.
(38) Soupart, A.; Alary, F.; Heully, J.-L.; Dixon, I. M. On the Possible Coordination on a ^{3}MC State Itself? Mechanistic Investigation Using DFT-Based Methods. *Inorganics* **2020**, *8*, 15.
(39) Soupart, A.; Alary, F.; Heully, J.-L.; Elliott, P. I. P.; Dixon, I. M. Theoretical Study of the Full Photosolvolysis Mechanism of $[Ru(bpy)_3]^{2+}$: Providing a General Mechanistic Roadmap for the Photochemistry of $[Ru(\hat{N}N)_3]^{2+}$-Type Complexes toward Both cis and trans Photoproducts. *Inorg. Chem.* **2020**, *59*, 14679−14695.
(40) Rode, B.; Schwenk, C.; Hofer, T.; Randolf, B. Coordination and Ligand Exchange Dynamics of Solvated Metal Ions. *Coord. Chem. Rev.* **2005**, *249*, 2993−3006.
(41) Moin, S. T.; Hofer, T. S.; Weiss, A. K. H.; Rode, B. M. Dynamics of Ligand Exchange Mechanism at Cu(II) in water: An Ab Initio Quantum Mechanical Charge Field Molecular Dynamics Study with Extended Quantum Mechanical Region. *J. Chem. Phys.* **2013**, *139*, 014503.

https://doi.org/10.1021/acs.jpclett.1c01424
J. Phys. Chem. Lett. 2021, 12, 7278−7284

(42) Hodel, F. H.; Deglmann, P.; Luber, S. Exploring Solvation Effects in Ligand-Exchange Reactions via Static and Dynamic Methods. *J. Chem. Theory Comput.* **2017**, *13*, 3348−3358.
(43) Sengupta, A.; Seitz, A.; Merz, K. M. Simulating the Chelate Effect. *J. Am. Chem. Soc.* **2018**, *140*, 15166−15169.
(44) Ahmadi, S.; Barrios Herrera, L.; Chehelamirani, M.; Hostaš, J.; Jalife, S.; Salahub, D. R. Multiscale Modeling of Enzymes: QM-cluster, QM/MM, and QM/MM/MD: A Tutorial Review. *Int. J. Quantum Chem.* **2018**, *118*, e25558.
(45) Moret, M.-E.; Tavernelli, I.; Rothlisberger, U. Combined QM/MM and Classical Molecular Dynamics Study of $[Ru(bpy)_3]^{2+}$ in Water. *J. Phys. Chem. B* **2009**, *113*, 7737−7744.
(46) Moret, M.-E.; Tavernelli, I.; Chergui, M.; Rothlisberger, U. Electron Localization Dynamics in the Triplet Excited State of $[Ru(bpy)_3]^{2+}$ in Aqueous Solution. *Chem. - Eur. J.* **2010**, *16*, 5889−5894.
(47) Tavernelli, I.; Curchod, B. F.; Rothlisberger, U. Nonadiabatic Molecular Dynamics with Solvent Effects: A LR-TDDFT QM/MM Study of Ruthenium (II) Tris(Bipyridine) in Water. *Chem. Phys.* **2011**, *391*, 101−109.
(48) Elian, M.; Hoffmann, R. Bonding Capabilities of Transition Metal Carbonyl Fragments. *Inorg. Chem.* **1975**, *14*, 1058−1076.
(49) Reinhard, M.; Auböck, G.; Besley, N. A.; Clark, I. P.; Greetham, G. M.; Hanson-Heine, M. W. D.; Horvath, R.; Murphy, T. S.; Penfold, T. J.; Towrie, M.; et al. Photoaquation Mechanism of Hexacyanoferrate(II) Ions: Ultrafast 2D UV and Transient Visible and IR Spectroscopies. *J. Am. Chem. Soc.* **2017**, *139*, 7335−7347.
(50) Schröder, D.; Shaik, S.; Schwarz, H. Two-State Reactivity as a New Concept in Organometallic Chemistry. *Acc. Chem. Res.* **2000**, *33*, 139−145.
(51) Neese, F. The ORCA Program System. *Wiley Interdiscip. Rev.: Comput. Mol. Sci.* **2012**, *2*, 73−78.
(52) Perdew, J. P.; Burke, K.; Ernzerhof, M. Generalized Gradient Approximation Made Simple. *Phys. Rev. Lett.* **1996**, *77*, 3865−3868.
(53) Adamo, C.; Barone, V. Toward Reliable Density Functional Methods Without Adjustable Parameters: The PBE0Models. *J. Chem. Phys.* **1999**, *110*, 6158−6170.
(54) Weigend, F.; Ahlrichs, R. Balanced Basis Sets of Split Valence, Triple Zeta Valence and Quadruple Zeta Valence Quality for H to Rn: Design and Assessment of Accuracy. *Phys. Chem. Chem. Phys.* **2005**, *7*, 3297−3305.
(55) Sinnecker, S.; Rajendran, A.; Klamt, A.; Diedenhofen, M.; Neese, F. Calculation of Solvent Shifts on Electronic g-Tensors with the Conductor-Like Screening Model (COSMO) and Its Self-Consistent Generalization to Real Solvents (Direct COSMO-RS). *J. Phys. Chem. A* **2006**, *110*, 2235−2245.
(56) Jónsson, H.; Mills, G.; Jacobsen, K. W. In *Classical and Quantum Dynamics in Condensed Phase Simulations*; Berne, B. J., Ciccotti, G., Coker, D. F., Eds.; World Scientific1998; Chapter 16, pp 385−404.
(57) Herbol, H. C.; Stevenson, J.; Clancy, P. Computational Implementation of Nudged Elastic Band, Rigid Rotation, and Corresponding Force Optimization. *J. Chem. Theory Comput.* **2017**, *13*, 3250−3259.
(58) Car, R.; Parrinello, M. Unified Approach for Molecular Dynamics and Density-Functional Theory. *Phys. Rev. Lett.* **1985**, *55*, 2471−2474.
(59) *CPMD*, version 3.15.1; IBM Corp. 1990−2008; MPI für Festkörperforschung: Stuttgart, Germany, 1997−2001. http://www.cpmd.org.
(60) Sit, P. H.-L.; Marzari, N. Static and Dynamical Properties of Heavy Water at Ambient Conditions from First-Principles Molecular Dynamics. *J. Chem. Phys.* **2005**, *122*, 204510.
(61) Nguyen, T. T.; Jung, J.; Trivelli, X.; Trébosc, J.; Cordier, S.; Molard, Y.; le Pollés, L.; Pickard, C. J.; Cuny, J.; Gautier, R. Evaluation of ^{95}Mo Nuclear Shielding and Chemical Shift of $[Mo_6X_{14}]^{2-}$ Clusters in the Liquid Phase. *Inorg. Chem.* **2015**, *54*, 7673−7683.
(62) Laasonen, K.; Car, R.; Lee, C.; Vanderbilt, D. Implementation of Ultrasoft Pseudopotentials in Ab Initio Molecular Dynamics. *Phys. Rev. B: Condens. Matter Mater. Phys.* **1991**, *43*, 6796−6799.
(63) Ceriotti, M.; Bussi, G.; Parrinello, M. Langevin Equation with Colored Noise for Constant-Temperature Molecular Dynamics Simulations. *Phys. Rev. Lett.* **2009**, *102*, 020601.

https://doi.org/10.1021/acs.jpclett.1c01424
J. Phys. Chem. Lett. 2021, 12, 7278−7284